Optical Materials 123 (2022) 111866

Contents lists available at ScienceDirect

Optical Materials

journal homepage: www.elsevier.com/locate/optmat

Efficient near infrared to visible light upconversion from Er/Yb codoped PVDF fibrous mats synthesized using a direct polymer doping technique

Saptasree Bose [a], Jack Ryan Summers [a], Bhupendra B. Srivastava [b], Victoria Padilla-Gainza [a], Manuel Peredo [a], Carlos Mauricio Trevino De Leo [c], Bryan Hoke [c], Santosh K. Gupta [d,e], Karen Lozano [a,*]

[a] Mechanical Engineering Department, University of Texas Rio Grande Valley, Edinburg, TX, 78539, USA
[b] Department of Chemistry, University of Texas Rio Grande Valley, Edinburg, TX, 78539, USA
[c] Department of Physics and Astronomy, University of Texas Rio Grande Valley, Brownsville, TX, 78520, USA
[d] Radiochemistry Division, Bhabha Atomic Research Centre, Trombay, Mumbai, 400085, India
[e] Homi Bhabha National Institute, Anushaktinagar, Mumbai, - 400094, India

ARTICLE INFO

Keywords:
Nanofibrous mat
Lanthanides
Forcespinning
Upconversion photoluminescence
Energy transfer

ABSTRACT

Upconverting-materials are capable of converting near infra-red (NIR) excitation into lower wavelengths. These materials could have a myriad of promising potential applications. However, in some areas, its use has been hindered by its low upconversion luminescence (UCL) efficiency and processing/handling disadvantages from luminescent materials in powder form. This work presents a step towards overcoming this limitation, by developing polymer-based fiber membranes without adding external luminescent powders. Herein, we report on the synthesis of Yb^{3+} and Er^{3+} codoped polyvinylidene difluoride (PVDF) and its development into fiber membranes using the Forcespinning® technique. X-ray diffraction (XRD), Fourier transformed infrared (FTIR) spectroscopy were performed to confirm the phase formation, crystallinity and the presence of vibrational bands of the corresponding PVDF matrix. Scanning Electron microscopy (SEM) and thermogravimetric analysis were conducted to investigate the morphological and thermal properties of the codoped nanofibers while the X-ray photoelectron spectroscopy (XPS) showed efficient doping of the lanthanides in the PVDF fiber. Under exposure to 980 nm NIR illumination, the PVDF:Yb^{3+},Er^{3+} fibrous mats exhibited efficient UCL emission in the visible wavelength region (523, 540 and 656 nm). The observed results show a NIR to visible UCL process where the Yb^{3+} ions act as the sensitizer for the generation of visible upconversion emission from Er^{3+} ions through an excited state absorption (ESA) and two photon energy transfer (ET) mechanisms. The developed material further opens potential lighting and imaging related applications given the ease of preparation, handling, and flexibility of the developed membranes.

1. Introduction

Upconvertible phosphor materials (UCPMs) have gained rising attention due to their unique photoluminescent properties of upconverting near-infrared light to a shorter wavelength of visible or ultraviolet (UV) radiation. UCPMs are showing strong potential applications in the areas of anti-counterfeiting, solar energy, bioimaging, security, optical communication, night vision, optoelectronics, etc. [1–4]. Near infrared (NIR) in particular, offers an advantage pertaining to in vivo and in vitro bioimaging applications, as compared to potentially harmful UV radiation, which is common in surgery. NIR has shown less tissue damage and has the ability to penetrate deeper into the tissue, also offers low autofluorescence [5]. Over the years extensive research in UCPMs has focused mainly on designing powder-based systems, such as, fluoride-based nano powder materials or nanoflourides, which are expected to offer a high upconversion yield, owing to low phonon energy and thus decrease of non-radiative channels. This makes powdered systems a popular topic for current literature pertaining to UCPMs. However, several disadvantages, including commercial viability, have been experienced when using powder based systems, such as: poor adhesion quality, low biocompatibility, poor thermal stability, low photostability, a tendency to aggregate, low mechanical strength,

* Corresponding author.
E-mail address: karen.lozano@utrgv.edu (K. Lozano).

https://doi.org/10.1016/j.optmat.2021.111866
Received 26 October 2021; Received in revised form 27 November 2021; Accepted 30 November 2021
Available online 4 December 2021

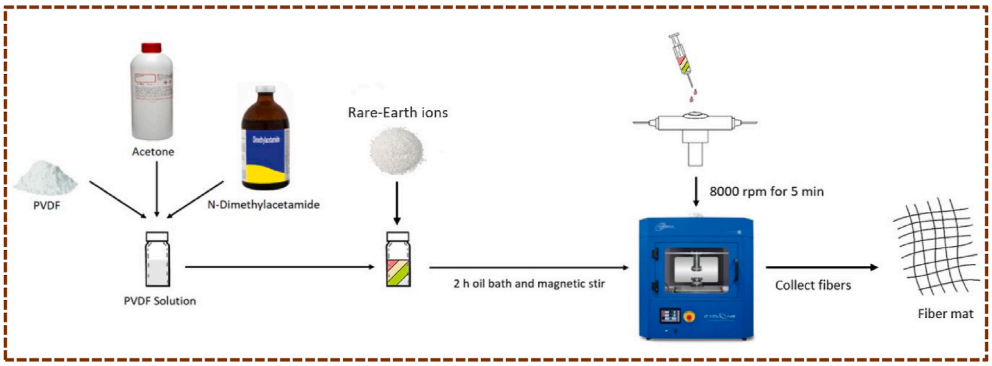

Scheme 1. Schematic representation for the synthesis of upconvertible PVDF fibrous mat.

restricted tuning capability, inability to get processed into other material forms, etc. [6–9]. Moreover, Direct doping of inorganic phosphors nanopowder leads to severe defects in the materials as a part of charge compensation, lattice strain owing to ionic radius mismatch and powder/crystals suffers from poor adhesion, lower flexibility, poor biocompatibility arising from solid powder curtailing its applicability to full potential [10–12]. Though, these issues have mostly been overlooked by academic publications, most of the published work is based on powder-based systems. The most significant drawbacks of nanofluorides are related to safety related issues when processing and inefficient performance under low laser power [1]. Moreover, nanofluorides have large surface defects which will adversely affect the performance of UCPMs due to the additional channels for non-radiative relaxations. Therefore, by replacing powder nanofluorides with a solution-processable fluorine-containing polymer, used as the UCL host, and in situ doped with rare-earth ions offers a significant advantage over powder systems alleviating current drawbacks of powder based systems. Additional benefits by using a fluorine host polymer includes ease of handling, improved flexibility, higher photostability, enhanced mechanical strength, diverse tunability, etc. [6,7,13]. The presence of fluorine atoms within the polymeric fibers also offer an advantage of low phonon energy and counterbalances the vibrations of lighter carbon and hydrogen atoms.

Our recent work has shown the capability of polymeric fibers in the area of optoelectronics, smart textiles, pressure sensors, etc. [6–8,14,15] Fibrous based membranes have shown improved luminescence quantum efficiency compared to powder-based systems, owing to better dispersion of phosphor particles in the former [6,14,15]. Al-Hossainy et al. have reported the effect of copper oxide nanoparticles on the optoelectronic properties of poly(o-anthranilic acid)-poly(o-amino phenol)/copper oxide nanocomposites based on their band gap and dispersion parameters [16]. Szczeszak et al. [17] have explored upconversion luminescence (UCL) in cellulose composites by encapsulating SrF_2: RE (rare-earth) nanopowder in the organic polymer. Similarly, Hou et al. [18] designed composite fibers for dual drug delivery system where upconversion core/shell silica nanoparticles were encapsulated within poly(ε-caprolactone)-gelatin based polymer matrix using the electrospinning technique. Liu and his group [19] developed electrospun $NaYF_4$:Ln^{3+} nanoparticle/polystyrene hybrid fibrous membranes for UCL analysis. Ge et al. [20] have also used the electrospinning method and explored one-dimensional $Yb_2Ti_2O_7$:Er nanofibers for UCL. Li and his colleagues [21] have synthesized microfibers consisting of upconversion nanoparticles (UCNPs) and polymethyl methacrylate (PMMA). None of these studies could achieve UCL without luminescent powders as nanofillers.

Here, we directly dope upconvertible rare-earth ions into the polymeric host without adding any external luminescent powder system. The selection of polymeric host is crucial for ultimate desired properties. It must be thermally/chemically stable, should prevent capturing visible photons, should possess wide optical transparency, optimum refractive index, etc. Some studies have presented work on the density functional theory calculations and optical dielectric constant analysis of polymeric systems and have highlighted its potential for optoelectronic applications [22–26]. Based on above mentioned work, polyvinylidene difluoride (PVDF, $C_2H_2F_2$) was selected as the semi-crystalline polymer host coupled with other advantages such as mechanical strength, thermal and chemical stability [7,8,13] as well as ease of processing into fiber form. Here we used the Forcespinning® (FS) method to prepare the fibers. This method presents several advantages over extensively explored electrospinning. Such as, no voltage is needed and the output is significantly higher with proven industrial production [13]. Its production rate is about 60 g/h for a lab-scale system while as for the industrial scale, the technology produces hundreds of meters per minute, with a controllable grams per square meter. The novel strategy of directly doping upconversion lanthanide couple Er^{3+}-Yb^{3+}directly into PVDF polymer and further ensemble them into fiber via FS technology opens a new research pathway in the area of UCPMs. The developed codoped PVDF based fiber membranes were thoroughly characterized using x-ray diffraction (XRD), thermogravimetric analysis (TGA), x-ray photoelectron spectroscopy (XPS), Fourier transformed infrared spectroscopy (FTIR) and field emission scanning electron microscopy (FESEM) as well as UCL and laser powder dependent UCL analysis.

2. Experimental

2.1. Materials

Polyvinylidene difluoride (PVDF), with an average molecular weight of 534000 $gmol^{-1}$ was procured from Arkema-Kynar. Erbium (III) nitrate pentahydrate ($Er(NO_3)_3{\cdot}5H_2O$), ytterbium (III) nitrate pentahydrate ($Yb(NO_3)_3{\cdot}5H_2O$), N, N-dimethylacetamide (≥99%, DMA) and acetone (≥99.5%) were purchased from Sigma-Aldrich and were used as received.

2.2. Synthesis

2.2.1. Synthesis of pure PVDF fibrous mats

The polymer solution was prepared by mixing 1.08 g of PVDF, 2 mL of DMA and 3 mL of acetone. Afterwards, the mixture was homogenized by a magnetic stirrer on a hot plate at 60 °C for 2 h. PVDF fibers were then produced using FS technology. A cylindrical spinneret coupled with 30 G needles was used within a Cyclone instrument (Fiberio Technologies, Inc). A 3 mL syringe was used to inject 2 mL of the solution into the spinneret and fibers were then extruded through two 30 G needles at 7000–8000 rpm for 8 min at an ambient temperature of 24 °C and relative humidity of 35–40%. Lastly, the fibers were gathered using a 10 cm × 10 cm aluminum frame collector from in between posts (Scheme 1).

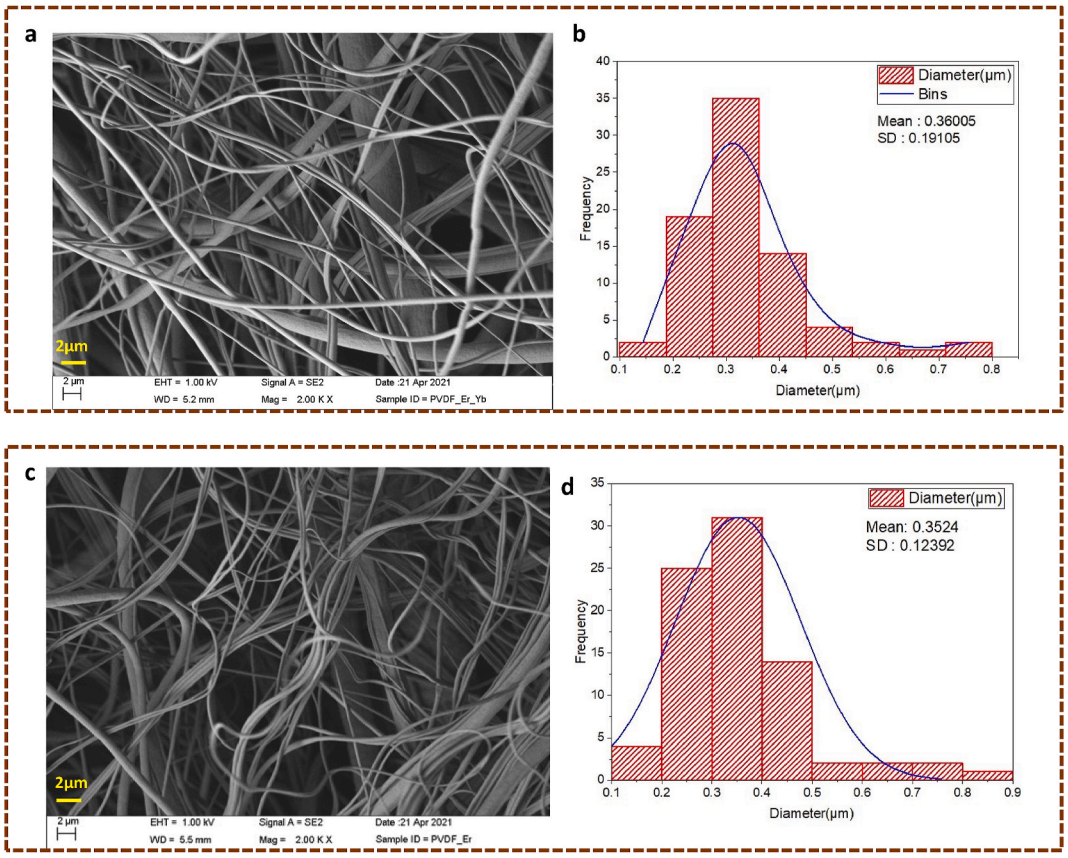

Fig. 1. SEM images and corresponding histograms for fiber diameters of the (a, b) Er/Yb-PVDF, (c, d) Er-PVDF.

2.2.2. *Synthesis of Er^{3+}/Yb^{3+} co-doped PVDF fibrous mats*

Erbium and Ytterbium co-doped PVDF fibrous mats were synthesized using $Er(NO_3)_3{\cdot}5H_2O$ and $Yb(NO_3)_3{\cdot}5H_2O$ salts (1:1.4) which were mixed with the polymer solution following the same procedure of fiber production described in the previous section. Other concentration ratios of activator (Er) and sensitizer (Yb) ions doped in the particular host were investigated (Er and Yb dopants (1:1; 1:1.4; 1:2.5; 1:3)), Er:Yb = 1 : 1.4 ratio shows the highest upconversion emission intensity. Beyond this concentration (Er:Yb = 1:1.4), a decrease in UCL emission takes place which might be attributed to an increased non-radiation emission within the system. All studies were performed using this optimum concentration. The doped sample containing only erbium was also synthesized.

2.3. *Instrumentation*

A scanning electron microscope (SEM) (Sigma VP; Carl Zeiss, Jena, Germany) was used to analyze the size and morphology of the generated fibers. The fibrous mats were gold sputtered before capturing the SEM images using a Denton Vacuum sputtering instrument. Developed fibers were also analyzed by a Thermo Scientific K-Alpha XPS with a 180° double focusing hemispherical analyzer and 128 channel detectors. The accuracy of the binding energy (BE) was 0.1 eV as calibrated by Cu $3P_{3/2}$ (75.1 eV) and Cu $2P_{3/2}$ (932.7 eV) reference peaks. Survey scan spectra of the fibrous mats were taken with 10 scans at a surface scan spot of 300 µm. Thermogravimetric analysis was conducted using a Netzsch TG 209 at a rate of 10 °C/min under N_2. Aluminum hermetic pans were used as sample holders, to contain 10 mg of the fiber mat. Fourier Transform Infrared (FTIR) spectra for the nanofibers were collected using a benchtop FTIR Nicolet iS 5 FTIR spectrometer by Thermo Scientific (by running the samples from 1500 to 600 cm^{-1}) and powder X-ray diffraction patterns of the nanofibers were recorded using a Bruker D8 Advance X-ray diffractometer (XRD) with Cu Kα1 radiation (λ = 0.15406 nm). XRD analysis was performed using a scanning mode of 2θ with a scanning step size of 0.04° and a scanning rate of 2.0° min^{-1} to quantify the phases of the PVDF fibers. Upconversion luminescence measurements were performed using an Edinburgh Instrument, a FLS 980 which was equipped with an MDL–III–980-2W Class IV laser.

3. Results and discussion

3.1. *Scanning electron microscopic (SEM) analysis*

Fig. 1 shows the representative SEM images of the as-produced Er–Yb co-doped (Fig. 1a) and Er doped (Fig. 1c) PVDF fibrous mats. The size distribution plot of PVDF:Yb,Er and PVDF:Er are shown respectively in Fig. 1b and d. The fibers are uniform in nature with lengths of up to several microns and the diameters mostly between 250 and 350 nm. Moreover, developed fibers show smooth surfaces without beads or fiber breakage, most of the fibers are observed to be long, continuous, and homogeneous.

3.2. *Powder X-Ray diffraction (PXRD) analysis*

XRD analysis was primarily carried out to focus on the crystalline α, β, and γ phases. Fig. 2 (a) shows the XRD pattern of pristine PVDF along with singly Er doped and Yb,Er co-doped PVDF fibers. For all developed systems, the most prominent peak is located around 20.6° which correlates with typical reflections of β phase in PVDF, corresponding to 110/200 reflection of the orthorhombic β phase [27,28]. Two weaker XRD peaks, at around 17.5° and 38.8° correspond to 020 and 211 reflections of monoclinic γ-phase PVDF. Additionally, there is a small component of monoclinic α phase corresponding to 35.5° which represents its 200 reflections. Doping with Er and Er/Yb did not cause a shift in the observed peaks. However, the intensity of β phase was higher for

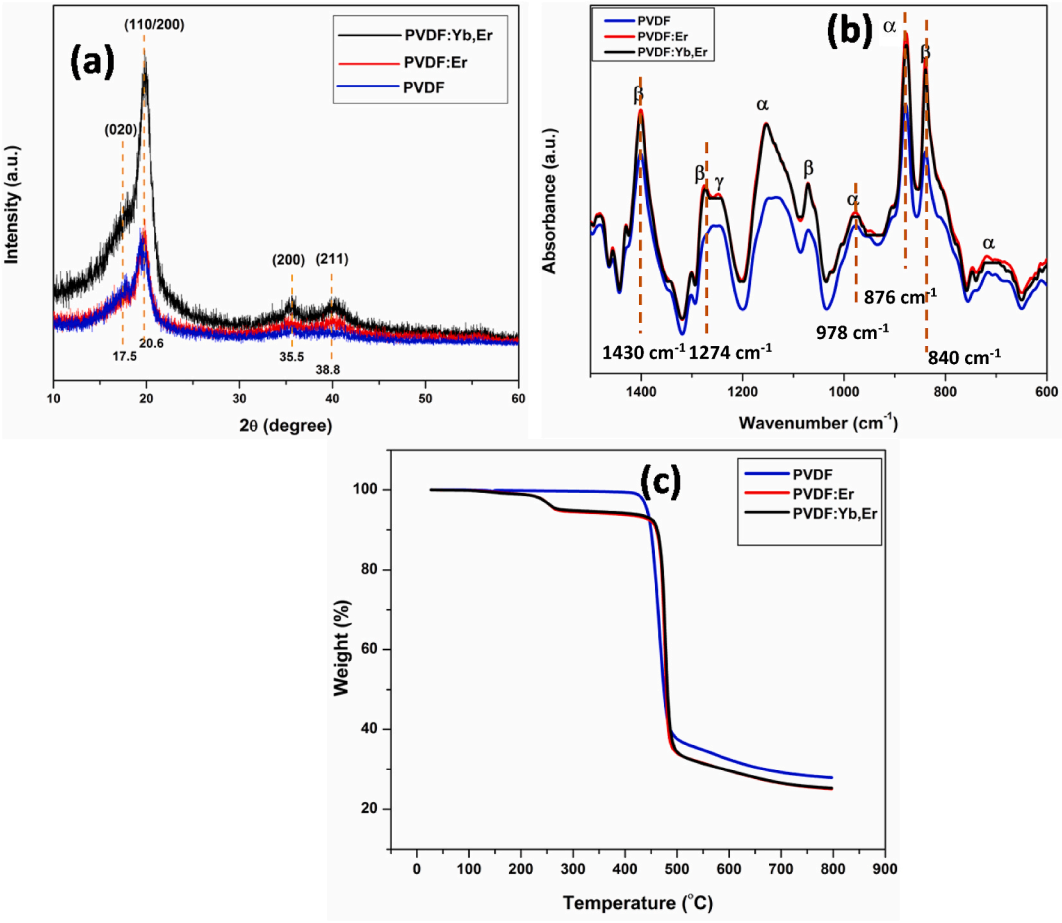

Fig. 2. (a) XRD, (b) FTIR and (c) TGA of pure PVDF, Er-PVDF, and Er/Yb-PVDF fibrous mats.

the rare-earth co-doped PVDF fibers.

3.3. Fourier transform infrared (FTIR) spectroscopic analysis

Fig. 2 (b) shows the FTIR spectra (1500–600 cm^{-1}) of the pure PVDF, Er-doped PVDF, and Er/Yb-co-doped PVDF fibers. The characteristic infrared (IR) absorption bands of the β-phase are observed at 840, 1274, and 1430 cm^{-1} for all the three samples. Moreover, the absorbance peaks located at 876 and 978 cm^{-1} are characteristic features for the non-polar α-phase [7,29,30]. The peaks corresponding to the α, β, and γ phases were also identified in the IR spectra. From the spectra it is clear that the predominant phase is the β phase, with only traces of α, and γ for all three samples. This is concurrent with the XRD results. It is clearly seen that on doping Er or co-doping of Er–Yb pair, the fractions of α, β and γ increase consistently. The intensities of the peaks are higher in the case of rare-earth doped PVDF nanofibers, than that of pure PVDF nanofibers, indicating that rare-earth ions contribute to the formation of the polar phase.

3.4. Thermogravimetric analysis (TGA)

Fig. 2c shows the TGA plot of pristine, Er^{3+}-doped, and Er^{3+}/Yb^{3+} co-doped PVDF fibers. The thermogram for undoped PVDF fiber mats shows ~62% loss at 422 °C, which indicates degradation of the PVDF polymer [31]. For the doped systems (Er^{3+} and Er^{3+}/Yb^{3+}), the spectra clearly show a two-step degradation process. The first step happens

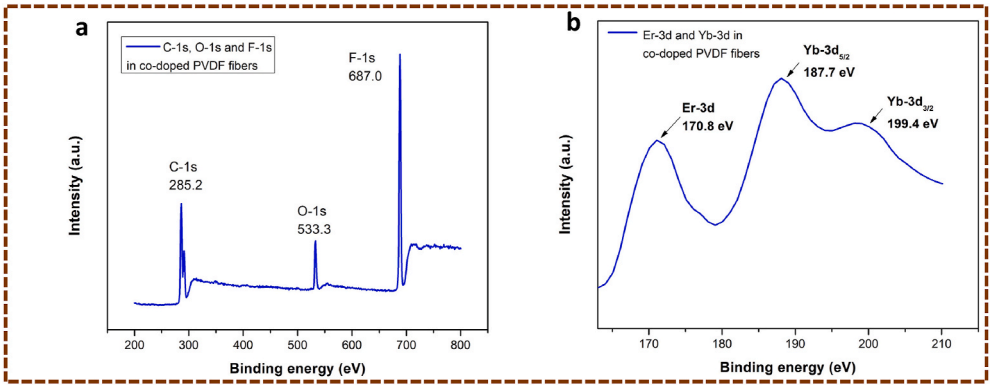

Fig. 3. XPS spectra of pure Er/Yb-PVDF fibrous mats.

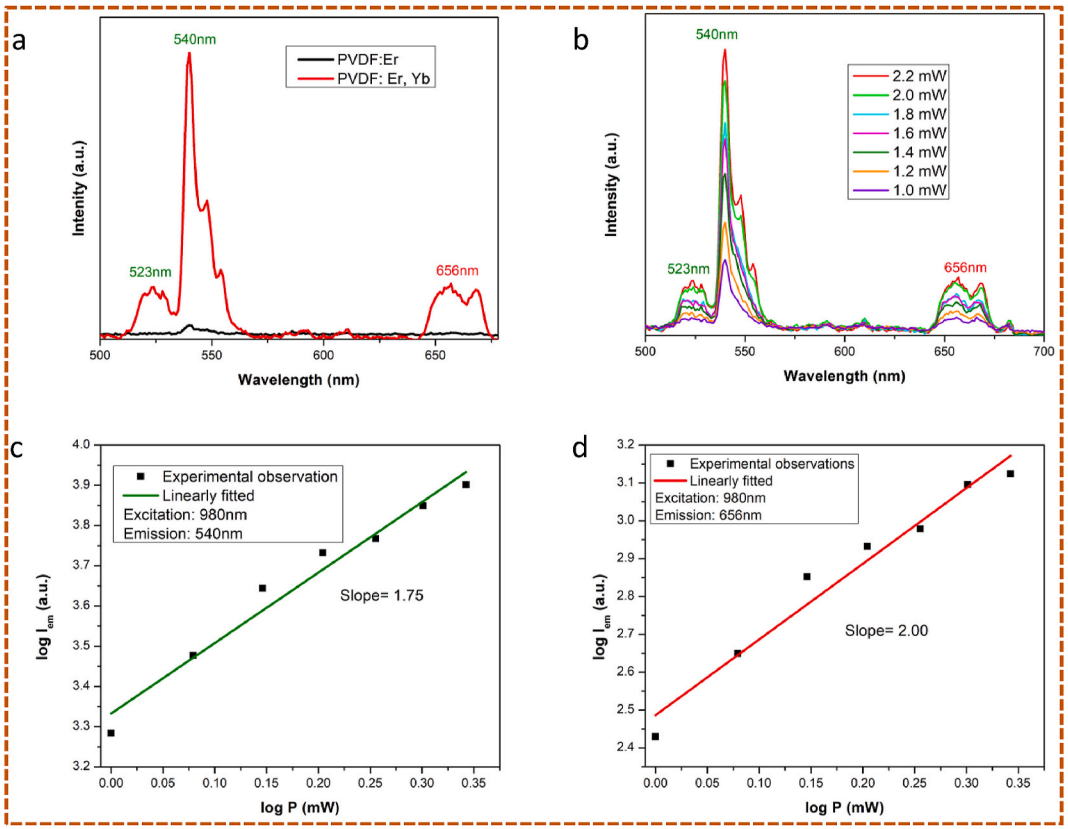

Fig. 4. (a) Upconversion photoluminescence of Er^{3+} doped and Er^{3+}/Yb^{3+} co-doped PVDF fibrous mat using 980 nm laser excitation source; (b) Upconversion photoluminescence intensity of co-doped sample (Er^{3+}: Yb^{3+} = 1:1.4) with different powers of the 980 nm laser excitation source; (c) The pump power dependence of upconversion visible photoluminescence intensity at 540 nm; (d) The pump power dependence of upconversion visible photoluminescence intensity at 656 nm.

around 215–225 °C and the second at 455–500 °C. The first one is attributed to the loss of crystal water molecules, which indicates that the crystal water present in the precursor rare-earth salts are introduced within the PVDF polymer matrix. The second loss is due to polymer degradation [31]. Doping the PVDF with Er–Yb results in a slight increase in thermal stability, possibly due to the interaction among PVDF polymeric chains and rare-earth ions.

3.5. X-ray photoelectron spectroscopy (XPS)

XPS results shown in Fig. 3 show the presence of carbon (1s), oxygen (1s), and fluorine (1s) atoms of the PVDF backbone with binding energies of 285.2, 533.3, and 687.0 eV respectively [7]. In Fig. 3a, it is observed that the O 1s peak is located at 533.3 eV, which corresponds to the lattice oxygen in the prepared sample. From Fig. 3b, XPS peaks of Er^{3+} 3d, Yb^{3+} $3d_{5/2}$ and $3d_{3/2}$ from the co-doped fibers appear at 170.8, 187.7 and 199.4 eV respectively confirming the doping of these ions in +3 oxidation states within the system [32,33].

3.6. UC photoluminescence

The Er^{3+}-Yb^{3+} pair has been used to improve the 980 nm photon absorption of Er^{3+} ions, which is attributed to the efficient sensitization by Yb^{3+} ions. As a result, promotion of Er^{3+} ions to upper energy levels takes place through a process known as energy transfer upconversion (ETU) [34]. Yb^{3+} ions are triggered by the certainty of having a single excited energy state ($^2F_{5/2}$) and thus exhibit a very strong and broad absorption band at 980 nm [35].

Fig. 4a shows the UCL spectra for both Er^{3+} doped and Er^{3+}/Yb^{3+}co-doped PVDF fibers in the spectral region between 450 and 750 nm. Though both samples show UCL with 980 nm excitation, the relative UC intensity from PVDF:Er is extremely feeble compared to PVDF:Er,Yb. This could be attributed to the poor absorption coefficient of Er^{3+} solely towards the 980 nm photons, owing to forbidden f-f transitions which highlight the importance of Yb^{3+}ion as a sensitizer to induce an efficient UCL. In the case of PVDF:Yb,Er fiber mats, high UCL intensity is observed because of the efficient absorption of 980 nm photons by Yb^{3+} ion. This causes an excitation of Yb^{3+} ions from a ground to excited state, which then transfers energy to a metastable state, as well as to Er^{3+} ground state and thereby exciting it to higher excited state. The UCL spectrum of PVDF:Yb,Er revealed a very strong emission band at 540 nm (1st green) and two comparatively weaker emission peaks located at 523 nm (2nd green) and 656 nm (red). The Upconversion photoluminescence at 523 nm, 540 nm and 656 nm were assigned respectively to the $^2H_{11/2} \rightarrow {}^4I_{15/2}$, $^4S_{3/2} \rightarrow {}^4I_{15/2}$ and $^4F_{9/2} \rightarrow {}^4I_{15/2}$ transitions [32, 36]. An interesting work composed of Er–Yb codoped $SrWO_4$ system shows two slightly visible blue upconversion emission peaks along with the strong green and red peaks [37]. However, the purpose of this present work focuses on upconverting 980 nm photons to green and red light and normally difficult to obtain blue emission and the same was true in this case as well. Hence, measurements were performed from 500 nm onwards.

To understand the UCL process and appearance of both green and red bands from the PVDF:Yb,Er fibrous mats and to further understand the number of the photons responsible for subsequent visible emission, the UCL spectra was monitored at different laser powers. Fig. 4b shows the UCL emission spectra of PVDF:Yb,Er under 980 nm NIR photon irradiation with different laser powers. No changes were observed in the UCL spectral profile with varying laser power. However, there is a substantial change in the emission intensity with monotonic increase, which is observed as the laser power increases. To determine the number of NIR photons involved in the $Yb^{3+} \rightarrow Er^{3+}$ energy transfer process, UCL

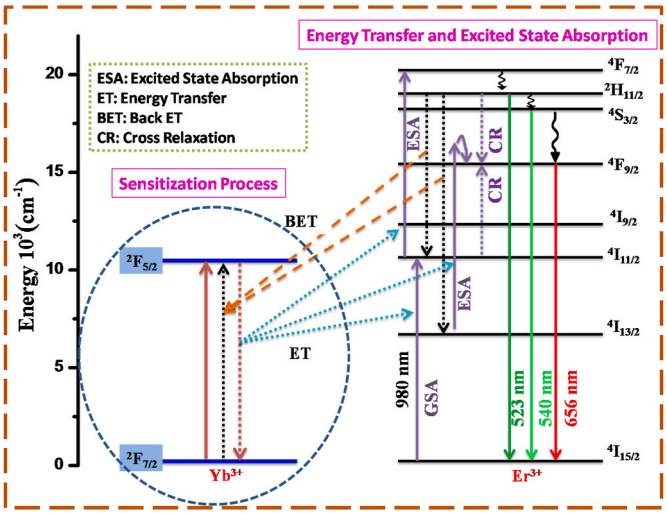

Fig. 5. UCL mechanism in PVDF:Yb,Er.

intensities were recorded at different laser powers. From this experiment the number of NIR photons can be obtained using following equation [38]:

$$I \alpha P^{n} \quad (1)$$

Where "I" is the UCL intensity, "*P*" is the laser power used, and "n" is the number of photons involved in the upconversion process. Fig. 4c and d demonstrate the double log graph of UCL intensity and laser power for green and red bands respectively. In both graphs there are linear trends with a slope of 1.75 for green and 2.00 for red, suggesting that UCL in the green and red regions for PVDF:Yb,Er fibrous mats are endowed by absorption of two NIR pump photons.

UCL is predominantly governed by two different photophysical processes, the ETU, and the excited state absorption (ESA). Other less known mechanisms viz. avalanche process or inter ion cross-relaxation are also reported [39]. ESA is normally the most sought out phenomenon for UCL, even in cases where only Erbium ions are used at low concentrations. Alternatively, ETU predominates for Yb–Er couples present in higher concentrations, as it proceeds through energy transfer between activator and sensitizer. Therefore, high concentrations of dopant ions could be avoided to minimize non-radiative relaxation channels via concentration quenching [40].

The energy level diagram of Er^{3+} and Yb^{3+} ions with the proposed UC processes of the PVDF:Yb,Er fibrous mat is shown in Fig. 5. The process is initiated by an efficient capture of 980 nm photons by Yb^{3+} ions, which then triggers its transition from ground to $^{2}F_{5/2}$ excited state. Afterwards, and depending on the lifetime of $^{2}F_{5/2}$ state; Yb^{3+} ion reverts to $^{4}I_{11/2}$ level of Er^{3+} ions, dissipating excess energy through ETU owing a close energy match for these two states. The second photon is captured sequentially, inducing an electronic transition from $^{4}I_{11/2}$ energy states to $^{4}F_{7/2}$ of Er^{3+}. Thereafter, excited electrons lying in the $^{4}F_{7/2}$ level undergo relaxation to lower levels, releasing 523 and 540 nm green photons respectively from the $^{2}H_{11/2}$ and $^{4}S_{3/2}$ states and red photons from the $^{4}F_{9/2}$ states.

Red photon emission from the $^{4}F_{9/2}$ state involved two distinct phenomena, (1) a nonradiative relaxation (NRR) via $^{4}S_{3/2} \rightarrow {}^{4}F_{9/2}$ transition and (2) population of $^{4}I_{13/2}$ energy states through NRR of $^{4}I_{11/2} \rightarrow {}^{4}I_{13/2}$ transition. This was followed by a promotion of excited state to $^{4}F_{9/2}$ level, either via energy transfer involving $^{2}F_{5/2}(Yb^{3+}) + {}^{4}I_{13/2}(Er^{3+}) \rightarrow {}^{2}F_{7/2}(Yb^{3+}) + {}^{4}F_{9/2}(Er^{3+})$ or excited state absorption process as photon $+ {}^{4}I_{13/2}(Er^{3+}) \rightarrow {}^{4}I_{15/2}(Er^{3+}) + {}^{4}F_{9/2}(Er^{3+})$ [41]. The crux of this work, direct doping, fiber development, and efficient NIR to visible UC is well represented and summarized in Scheme 2.

4. Conclusion

In this work to overcome the limitations observed when using UCL phosphors in powder form and to increase the commercial viability of NIR to visible light emission systems, we have designed a novel rare earth doped polymeric based fiber membrane. A unique design strategy has been adopted wherein Yb^{3+} and $Er^{3+}$are directly doped inside the PVDF polymer host without adding luminescent nanocrystals, as conducted in previously reported studies. Furthermore, the system was produced using the FS technology which offers immediate access to industrial level finer fiber production. Designed PVDF:Yb,Er fibrous mats were thoroughly characterized using XRD, FTIR, XPS, TGA and FESEM. XRD and FTIR studies confirm the presence of higher beta fraction, compared to the monoclinic alpha and gamma phases, this is observed in both pristine and Yb–Er co-doped PVDF, with the latter revealing a higher yield of beta phase. Efficient doping and high purity of the fiber is confirmed using XPS. A fine and smooth texture of the fibrous mats, without beads; defect or blister formation was clearly demonstrated by FESEM morphostructural analysis. Moreover, doping of rare earth ions did not affect the thermal stability of the PVDF based fibrous mats. Efficient NIR to visible photon upconversion was seen in

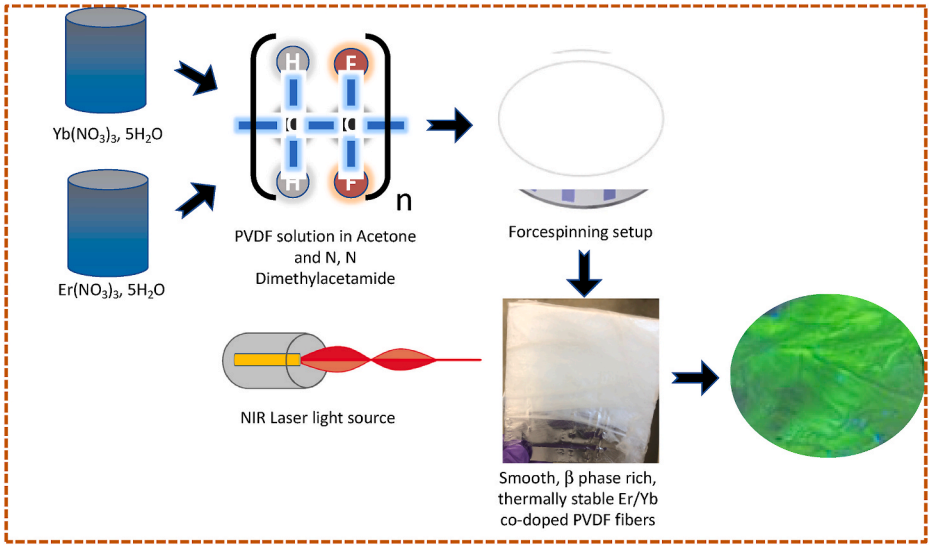

Scheme 2. Schematic showing direct doping, fiber development and effective upconversion luminescence of novel PVDF:Yb,Er fibrous mats.

PVDF:Yb,Er fibrous mats, this mechanism was well explained through ETU and ESA. Pump power dependent UCL measurements revealed 2-photon absorption for both green and red emissions. This work clearly demonstrated the potential of 1D PVDF polymeric fibers produced by the centrifugal spinning process as prospective host candidate with appropriate phonon energy to accommodate Er^{3+}/Yb^{3+} pair and to directly show successful UC photoluminescence. These results can be useful for future generation security lighting, solar energy, night vision and bioimaging applications.

CRediT authorship contribution statement

Saptasree Bose: Conceptualization, Methodology, Investigation, Data curation, Formal analysis, Visualization, Writing – review & editing. **Jack Ryan Summers:** Methodology, Investigation, Writing – review & editing. **Bhupendra B. Srivastava:** Methodology, Investigation, Data curation, Writing – review & editing. **Victoria Padilla-Gainza:** Methodology, Investigation. **Manuel Peredo:** Methodology, Investigation. **Carlos Mauricio Trevino De Leo:** Methodology, Investigation. **Bryan Hoke:** Methodology, Investigation. **Santosh K. Gupta:** Writing – review & editing. **Karen Lozano:** Conceptualization, Supervision, Visualization, Writing – review & editing.

Declaration of competing interest

The authors declare that they have no known competing financial interests or personal relationships that could have appeared to influence the work reported in this paper.

Acknowledgement

The authors acknowledge support received from National Science Foundation under PREM grant DMR 2122178.

References

[1] S.K. Gupta, K. Sudarshan, R.M. Kadam, Optical nanomaterials with focus on rare earth doped oxide: a Review, Mater. Today Commun. 27 (2021) 102277.
[2] Y. Wu, J. Xu, X. Qin, J. Xu, X. Liu, Dynamic upconversion multicolour editing enabled by molecule-assisted opto-electrochemical modulation, Nat. Commun. 12 (2021) 2022.
[3] Z. Zhang, Q. Han, J.W. Lau, B. Xing, Lanthanide-doped upconversion nanoparticles meet the needs for cutting-edge bioapplications: recent progress and perspectives, ACS Mater. Lett. 2 (2020) 1516–1531.
[4] X. Zheng, R.K. Kankala, C.-G. Liu, S.-B. Wang, A.-Z. Chen, Y. Zhang, Lanthanides-doped near-infrared active upconversion nanocrystals: upconversion mechanisms and synthesis, Coord. Chem. Rev. 438 (2021) 213870.
[5] S.K. Gupta, M.A.P. Garcia, J.P. Zuniga, M. Abdou, Y. Mao, Visible and ultraviolet upconversion and near infrared downconversion luminescence from lanthanide doped La2Zr2O7 nanoparticles, J. Lumin. 214 (2019) 116591.
[6] R. Barbosa, S.K. Gupta, B.B. Srivastava, A. Villarreal, H. De Leon, M. Peredo, S. Bose, K. Lozano, Bright and persistent green and red light-emitting fine fibers: a potential candidate for smart textiles, J. Lumin. 231 (2021) 117760.
[7] C. Hernandez, S.K. Gupta, J.P. Zuniga, J. Vidal, R. Galvan, H. Guzman, L. Chavez, K. Lozano, Y. Mao, High pressure responsive luminescence of flexible Eu3+ doped PVDF fibrous mats, J. Mater. Sci. Technol. 66 (2021) 103–111.
[8] C. Hernandez, S.K. Gupta, J.P. Zuniga, J. Vidal, R. Galvan, M. Martinez, H. Guzman, L. Chavez, Y. Mao, K. Lozano, Performance evaluation of Ce3+ doped flexible PVDF fibers for efficient optical pressure sensors, Sens. Actuators, A 298 (2019) 111595.
[9] M. Valdez, S.K. Gupta, K. Lozano, Y. Mao, ForceSpun polydiacetylene nanofibers as colorimetric sensor for food spoilage detection, Sensor. Actuator. B Chem. 297 (2019) 126734.
[10] B.B. Srivastava, S.K. Gupta, R. Barbosa, A. Villarreal, K. Lozano, Y. Mao, Rare earth free bright and persistent white light emitting zinc gallo-germanate nanosheets: technological advancement to fibers with enhanced quantum efficiency, Materials Advances 2 (2021) 4058–4067.
[11] S.K. Gupta, R.M. Kadam, P.K. Pujari, Lanthanide spectroscopy in probing structure-property correlation in multi-site photoluminescent phosphors, Coord. Chem. Rev. 420 (2020) 213405.
[12] P.-C. Jhang, Y.-C. Yang, Y.-C. Lai, W.-R. Liu, S.-L. Wang, A fully integrated nanotubular yellow-green phosphor from an environmentally friendly eutectic solvent, Angew. Chem. Int. Ed. 48 (2009) 742–745.
[13] S.K. Gupta, C. Hernandez, J.P. Zuniga, K. Lozano, Y. Mao, Luminescent PVDF nanocomposite films and fibers encapsulated with $La_2Hf_2O_7:Eu^{3+}$ nanoparticles, SN Applied Sciences 2 (2020) 616.
[14] S.S.H. Abir, S.K. Gupta, A. Ibrahim, B.B. Srivastava, K. Lozano, Tunable $CsPb(Br/Cl)_3$ perovskite nanocrystals and further advancement in designing light emitting fiber membranes, Mater. Adv. 2 (2021) 2700–2710.
[15] B.B. Srivastava, S.K. Gupta, R. Barbosa, A. Villarreal, K. Lozano, Y. Mao, Rare earth free bright and persistent white light emitting zinc gallo-germanate nanosheets: technological advancement to fibers with enhanced quantum efficiency, Mater. Adv. 2 (2021) 4058–4067.
[16] A.F. Al-Hossainy, M. Bassyouni, M.S. Zoromba, Elucidation of electrical and optical parameters of poly(o-anthranilic acid)-poly(o-amino phenol)/copper oxide nanocomposites thin films, J. Inorg. Organomet. Polym. Mater. 28 (2018) 2572–2583.
[17] A. Szczeszak, M. Skwierczyńska, D. Przybylska, M. Runowski, E. Śmiechowicz, A. Erdman, O. Ivashchenko, T. Grzyb, S. Lis, P. Kulpiński, K. Olejnik, Upconversion luminescence in cellulose composites (fibres and paper) modified with lanthanide-doped SrF2 nanoparticles, J. Mater. Chem. C 8 (2020) 11922–11928.
[18] Z. Hou, X. Li, C. Li, Y. Dai, P.a. Ma, X. Zhang, X. Kang, Z. Cheng, J. Lin, Electrospun upconversion composite fibers as dual drugs delivery system with individual release properties, Langmuir 29 (2013) 9473–9482.
[19] K.-C. Liu, Z.-Y. Zhang, C.-X. Shan, Z.-Q. Feng, J.-S. Li, C.-L. Song, Y.-N. Bao, X.-H. Qi, B. Dong, A flexible and superhydrophobic upconversion-luminescence membrane as an ultrasensitive fluorescence sensor for single droplet detection, Light Sci. Appl. 5 (2016) e16136-e16136.
[20] W. Ge, J. Shi, M. Xu, X. Chen, J. Zhu, Red upconversion luminescence (UCL) properties in one-dimensional $Yb_2Ti_2O_7$:Er nanofibers via an electrospinning route, J. Alloys Compd. 788 (2019) 993–999.
[21] H. Li, X. Sun, M.K. Shahzad, L. Liu, Facile preparation of upconversion microfibers for efficient luminescence and distributed temperature measurement, J. Mater. Chem. C 7 (2019) 7984–7992.
[22] A.A.I. Abd-Elmageed, S.M. Ibrahim, A. Bourezgui, A.F. Al-Hossainy, Synthesis, DFT studies, fabrication, and optical characterization of the [ZnCMC]TF polymer (organic/inorganic) as an optoelectronic device, New J. Chem. 44 (2020) 8621–8637.
[23] M.R. Eid, A.F. Al-Hossainy, Combined Experimental Thin Film, DFT-TDDFT Computational Study, Flow and Heat Transfer in [PG-MoS2/ZrO2]C Hybrid Nanofluid, Waves in Random and Complex Media, 2021, pp. 1–26.
[24] A.F. Al-Hossainy, M.R. Eid, Combined experimental thin films, TDDFT-DFT theoretical method, and spin effect on [PEG-H2O/ZrO2+MgO]h hybrid nanofluid flow with higher chemical rate, Surf. Interfaces 23 (2021) 100971.
[25] A.F. Al-Hossainy, A. Ibrahim, Structural, optical dispersion and dielectric properties of novel chromium nickel organic crystalline semiconductors, Mater. Sci. Semicond. Process. 38 (2015) 13–23.
[26] A.F. Al-Hossainy, A. Ibrahim, M.S. Zoromba, Synthesis and characterization of mixed metal oxide nanoparticles derived from Co–Cr layered double hydroxides and their thin films, J. Mater. Sci. Mater. Electron. 30 (2019) 11627–11642.
[27] X. Cai, T. Lei, D. Sun, L. Lin, A critical analysis of the α, β and γ phases in poly (vinylidene fluoride) using FTIR, RSC Adv. 7 (2017) 15382–15389.
[28] J.E. Trevino, S. Mohan, A.E. Salinas, E. Cueva, K. Lozano, Piezoelectric properties of PVDF-conjugated polymer nanofibers, J. Appl. Polym. Sci. 138 (2021) 50665.
[29] X. Liu, J. Ma, X. Wu, L. Lin, X. Wang, Polymeric nanofibers with ultrahigh piezoelectricity via self-orientation of nanocrystals, ACS Nano 11 (2017) 1901–1910.
[30] Y.K. Fuh, Z.M. Huang, B.S. Wang, S.C. Li, Self-powered active sensor with concentric topography of piezoelectric fibers, Nanoscale Res. Lett. 12 (2017) 44.
[31] Y. Sui, H. Luo, M.-M. Xing, Y. Zhu, F.-X. Zeng, Dielectric, ferroelectric, and photoluminescent properties of Dy3+ doped flexible multifunctional PVDF films, Ferroelectrics 520 (2017) 212–223.
[32] D. Haldar, A. Ghosh, U.K. Ghorai, S.K. Saha, Near infrared to visible upconversion photoluminescence from Er/Yb co-doped MoS2 nanosheets with tunable thickness, Mater. Res. Bull. 129 (2020) 110879.
[33] G. Bai, Z. Yang, H. Lin, W. Jie, J. Hao, Lanthanide Yb/Er co-doped semiconductor layered WSe2 nanosheets with near-infrared luminescence at telecommunication wavelengths, Nanoscale 10 (2018) 9261–9267.
[34] R.V. Perrella, I.C. Ribeiro, P.H.A. Campos-Junior, M.A. Schiavon, E. Pecoraro, S.J. L. Ribeiro, J.L. Ferrari, $CaTiO_3:Er^{3+}:Yb^{3+}$ upconversion from 980 nm to 1550 nm excitation and its potential as cells luminescent probes, Mater. Chem. Phys. 223 (2019) 391–397.
[35] X.X. Yang, Z.L. Fu, Y.M. Yang, C.P. Zhang, Z.J. Wu, T.Q. Sheng, Optical temperature sensing behavior of high-efficiency upconversion: Er_{3b}-Yb_{3b} Co-Doped $NaY(MoO_4)_2$ phosphor, J. Am. Ceram. Soc. 98 (2015) 2595–2600.
[36] C. Perez-Rodriguez, S. Rios, I.R. Martin, L.L. Martin, P. Haro-Gonzalez, D. Jaque, Upconversion emission obtained in Yb3+-Er3+ doped fluoroindate glasses using silica microspheres as focusing lens, Opt Express 21 (2013) 10667–10675.
[37] A. Pandey, V.K. Rai, V. Kumar, V. Kumar, H.C. Swart, Upconversion based temperature sensing ability of Er3+–Yb3+codoped SrWO4: an optical heating phosphor, Sensor. Actuator. B Chem. 209 (2015) 352–358.
[38] F. Vetrone, J.-C. Boyer, J.A. Capobianco, A. Speghini, M. Bettinelli, Significance of Yb^{3+} concentration on the upconversion mechanisms in codoped $Y_2O_3:Er^{3+}$, Yb^{3+} nanocrystals, J. Appl. Phys. 96 (2004) 661–667.

[39] G. Lakshminarayana, E.M. Weis, A.C. Lira, U. Caldiño, D.J. Williams, M.P. Hehlen, Cross Relaxation in rare-earth-doped oxyfluoride glasses, J. Lumin. 139 (2013) 132–142.

[40] C. Mi, J. Wu, Y. Yang, B. Han, J. Wei, Efficient upconversion luminescence from $Ba_5Gd_8Zn_4O_{21}$:Yb^{3+}, Er^{3+} based on a demonstrated cross-relaxation process, Sci. Rep. 6 (2016) 22545.

[41] Y. Yang, Z. Yang, P. Li, X. Li, Q. Guo, B. Chen, Dependence of optical properties on the composition in Er^{3+}-doped $xNaPO_3$–$(80-x)TeO_2$–$10ZnO$–$10Na_2O$ glasses, Opt. Mater. 32 (2009) 133–138.